OPEN ACCESS

University of BRISTOL

Peer reviewed version

Link to published version (if available):
10.1021/jp5014863

Link to publication record in Explore Bristol Research
PDF-document

Deviations from Plane-Wave Mie Scattering and Precise Retrieval of Refractive Index for a Single Spherical Particle in an Optical Cavity

Bernard J. Mason, Jim S. Walker, Jonathan P. Reid and Andrew J. Orr-Ewing*

School of Chemistry, University of Bristol, Bristol BS8 1TS, UK

Tel: 44 (0)117 9287672

e-mail: a.orr-ewing@bristol.ac.uk

Abstract

The extinction cross sections of individual, optically confined aerosol particles with radii of a micron or less can, in principle, be measured using cavity ring-down spectroscopy (CRDS). However, when the particle radius is comparable in magnitude to the wavelength of light stored in a high-finesse cavity, the phenomenological cross-section retrieved from a CRDS experiment depends on the location of the particle in the intra-cavity standing wave and differs from the Mie scattering cross section for plane-wave irradiation. Using an evaporating 1,2,6-hexanetriol particle of initial radius ~1.75 μm confined within the 4.5-μm diameter core of a Bessel beam, we demonstrate that the scatter in the retrieved extinction efficiency of a single particle is determined by its lateral motion, which spans a few wavelengths of the intra-cavity standing wave used for CRDS measurements. Fits of experimental measurements to Mie calculations, modified to account for the intra-cavity standing wave, allow precise retrieval of the refractive index of 1,2,6-hexanetriol particles (with relative humidity, RH < 10%) of 1.47824 $\pm$ 0.00072.

Keywords

Aerosol particle; Mie Scattering; Cavity Ring-Down Spectroscopy; Refractive Index; Accumulation Mode; Intra-Cavity Standing Wave.

1. Introduction

The magnitudes of the direct and indirect effects of atmospheric aerosol on scattering and absorption of solar radiation continue to contribute significant uncertainties to assessment of radiative forcing of the Earth's atmosphere.[1] Reduction of these uncertainties requires improved methods of laboratory determination of the optical properties of aerosol particles and their change with ambient relative humidity or oxidative chemical processing. Studies on single particles, confined within optical or electrodynamic traps, now provide precise measurements of aerosol refractive indices and phases, hygroscopic growth, evaporation of semi-volatile components, and other properties of importance for their atmospheric behaviour.[2-6] These trapping-based techniques are most applicable to single particles with radii greater than 1 μm, but the smaller accumulation mode particles are of greater significance for atmospheric processes.[4]

In a recent publication, we demonstrated that absolute extinction cross sections for single sub-micron radius spherical aerosol particles can be measured with high precision by combining optical confinement and levitation of a particle with cavity ring-down spectroscopy (CRDS).[7] The change in ring-down time (RDT) when a particle is moved from well below the optical axis (z) of the ring-down cavity (RDT = τ_0) to the height of the centre axis of the Gaussian TEM$_{00}$ cavity mode (RDT = τ) is given by:[8]

$$\frac{1}{\tau} - \frac{1}{\tau_0} = \frac{2c\sigma}{\pi L w^2} \tag{1}$$

Here, w is the beam waist of the cavity mode at the location of the particle, L is the length of the cavity, c is the speed of light and σ is a phenomenological extinction cross section deduced from the experimental measurements. If the particle position deviates by a radial distance R from the centre axis of the Gaussian TEM$_{00}$ mode, the measured extinction is smaller by a factor of $exp(-2R^2/w_0^2)$ than the value on-axis.[8] Fine control over the position of the trapped particle with respect to the centre of the TEM$_{00}$ mode was therefore implemented by confining the particle within a Bessel beam (BB) with a 4.5-μm diameter core that propagated vertically (defining our x coordinate). The particle position within the TEM$_{00}$ mode of the horizontally propagating CRD beam was controlled either by varying the height of the particle (i.e., the axial position x of the particle in the BB) or by moving the particle horizontally by translating the BB orthogonally to the CRD axis (along a coordinate denoted as y).

In the current study, we report observations of the evaporation of a droplet of a semi-volatile organic liquid, 1,2,6-hexanetriol by measurement of changes in extinction cross section with time. We also account quantitatively for scatter in the experimental data by treatment of the interaction

of the particle with the standing wave of the intra-cavity probe laser beam as the particle undergoes Brownian motion within the spatially confining core of the BB. Data analysis incorporating this latter effect provides a precise determination of the refractive index of the droplet.

2. Extinction cross section determination in an optical cavity

For experimental measurements of single-particle optical properties, we used the same apparatus as in our previous study,[7] which is illustrated schematically in figure 1. The figure also defines our choice of x, y and z coordinates. Radiation pressure from the trapping Bessel beam opposed the downward forces from gravity (insignificant for the small particles used in this work) and the drag force from a regulated gas flow. Feedback control of the laser beam power maintained the particle on the TEM_{00} mode axis while it underwent size reduction associated with evaporative loss of a semi-volatile component.
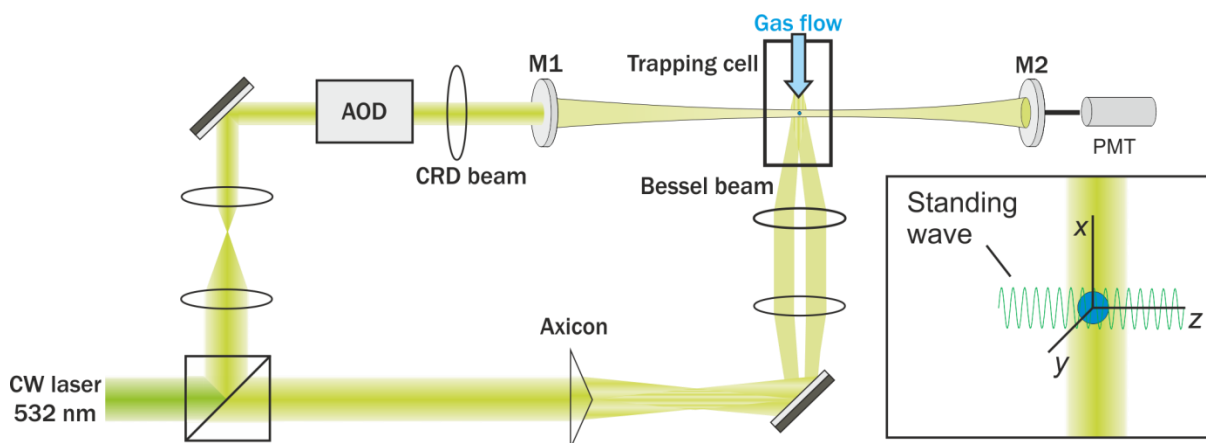

Figure 1: The combined Bessel beam and CRDS apparatus. M1 and M2 denote cavity end mirrors, AOD is an acousto-optic deflector and PD is a photodiode. The inset shows an enlarged view of the overlap of the CRDS and Bessel beams, a trapped aerosol particle, and the coordinate system used in the text.

If the spherical particle were illuminated by travelling plane wave radiation, the value of σ retrieved from equation (1) would correspond to the extinction cross section for Mie scattering, σ_{ext}. This parameter is intrinsic to the particle, and is determined by its size and composition.   Its measurement should not depend on the particle's axial (z) location in the ring-down cavity, provided the known change in beam waist with distance from the cavity end mirrors[9] is correctly treated in equation (1).   For plane wave illumination, the extinction cross section of the particle is related to its geometric cross section ($\sigma_{geom}=\pi r^2$ for a particle of radius r) by $\sigma_{ext} = Q_{ext}\sigma_{geom}$. The extinction

efficiency, Q_{ext} depends upon the refractive index of the particle ($m = n + ik$, with n and k the real and imaginary components, respectively) and the size parameter, $x_p = 2\pi r/\lambda$, which is the ratio of the particle circumference to the wavelength of the light (λ). However, the light trapped within an optical cavity forms a standing wave along the cavity axis z which can be described by two counter-propagating plane waves. Miller and Orr-Ewing[10] previously obtained a theoretical expression for the modification to the measured extinction coefficient that connects the scattering of a standing wave to plane wave Mie scattering. When the particle radius is comparable to the wavelength of the light, the experimentally determined phenomenological cross section of equation (1) depends on the axial location of the centre of the particle, and specifically, whether the particle's centre is coincident with a node, an extremum (anti-node) or some intermediate portion of the standing wave.

Miller and Orr-Ewing defined a phase parameter $\zeta(z)$ which modifies the Mie extinction cross section to account correctly for the effect of the standing wave structure on measurements in a ring-down cavity. The true Mie extinction cross section (σ_{ext}) and the phenomenological value derived from the CRDS measurement are related by:

$$\sigma = \zeta(z)\sigma_{ext} \qquad\qquad\qquad (2)$$

The phase parameter depends on the size parameter and refractive index, and a method for calculation of $\zeta(z)$ was reported previously.[10] Figure 2 compares the variation in $\zeta(z)$ for a particle centred at an extremum of the intra-cavity standing wave ($z = 0$) and at a node ($z = \lambda/4$). Between these limits, $\zeta(z)$ takes intermediate values and, thus, the two lines in fig 2 represent the limiting deviations from Mie scattering. At $z = \lambda/8$ the phase parameter $\zeta = 1$ for all size parameters. The calculation in figure 2 used a real refractive index $m = 1.48$ corresponding to a dry 1,2,6-hexanetriol droplet.
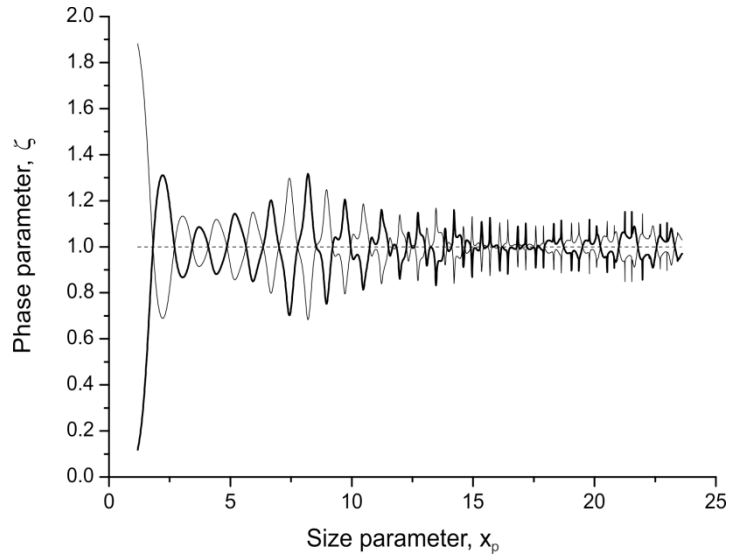
Figure 2: Calculated phase parameter ζ plotted as a function of size parameter for a particle centred either at a node (thinner line) or a maximum (thicker line) of the intra-cavity standing wave. The calculation was performed for a 1,2,6-hexanetriol droplet of refractive index m =1.48 and the wavelength of the standing wave was 532 nm.

3. Extinction efficiency changes for an evaporating 1,2,6-hexanetriol droplet

Figure 3 shows the values of the extinction efficiency for a dry 1,2,6-hexanetriol droplet undergoing evaporation, estimated from the measured fluctuations in RDT. The particle was held centrally in the ring-down cavity TEM$_{00}$ mode both radially (along x and y) and longitudinally (along z) using a 4.5 μm diameter Bessel beam core. Both the Bessel and the CRDS beams were generated from 532-nm wavelength light from a Coherent Verdi single mode continuous wave (cw) laser, as described previously.[7] A flow of dry nitrogen gas maintained a low relative humidity (RH < 10%) in the cell surrounding the trapping region. RDT measurements, from which Q_{ext} values were deduced, were made at a rate of ~10 ring down events per second. Phenomenological extinction cross sections were calculated from observed changes in RDT using equation (1), and converted to Q_{ext} values by dividing by geometric cross-sections. The particle radius was obtained from the analysis of interference fringes for light scattered from the trapping laser and collected over a known angular range (the phase function).[11-13] In the analysis described in section 5, the beam waist of the TEM$_{00}$ mode was obtained as 279 μm, which compares well to the value expected for our design of linear optical cavity of 272 μm.[9] Experimental measurements are overlaid by Mie scattering calculations in Figure 3 (dashed line) for particles in the size parameter range x_p = 10 to 21. The agreement indicates that the CRDS measurements return absolute extinction efficiency values and their

dependence on x_p with reasonable accuracy when processed in this way, and that the refractive index of the 1,2,6-hexanetriol droplet is correctly accounted for in the simulation. The solid lines in the figure derive from a more complete analysis that is discussed in sections 4 and 5.
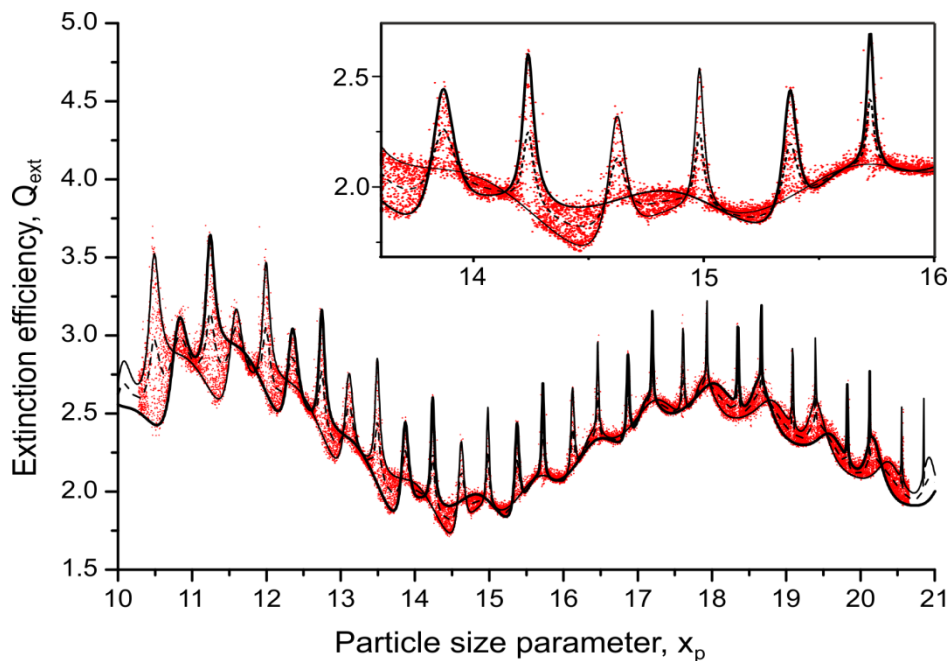

Figure 3: The main panel compares Q_{ext} data obtained from CRDS measurements for an evaporating 1,2,6-hexanetriol particle (red dots) with predictions from a standard Mie calculation (dashed line) with RI $m = 1.47748$. The inset shows an expanded view. The solid curves were obtained by modifying the Mie scattering cross section in accord with equation (2) to account for the measurement of extinction by light scattering within an optical cavity. The thicker and thinner lines correspond respectively to a particle centred at a maximum or a node of the intra-cavity standing wave.

4. Quantitative analysis of the distribution of experimental Q_{ext} values

The scatter of the CRDS measurements about the Mie theory curve merits further consideration. One possible cause of this distribution of experimental values is that the particle was undergoing fluctuations in its vertical position in the Bessel beam trap, resulting in measurements at different values of the vertical displacement from the central axis of the TEM_{00} mode. However, the data were obtained with tight feedback control of the laser power to maintain the central position of the particle. Camera observations indicated that the maximum vertical displacement during an entire set of measurements was ~20 μm. This maximum amplitude gives at most a 1 % change in the retrieved extinction cross-section. More representative displacements over timescales on which

fluctuations in ring down events are seen are typically less than 5 μm, corresponding to a 0.07 % change in the measured extinction cross-section. This variation is much smaller than the fluctuations evident in figure 3. The vertical excursions of the particle are therefore deduced to be sufficiently small not to contribute significantly to the envelope of data points seen in figure 3.

The scatter of the data points is more pronounced in proximity to resonances in the light scattering, and there are particular values of the droplet radius where the scattering in the range of measured Q_{ext} values is narrower. The explanation for these observations lies in the random motion of the particles orthogonal to the propagation axis of the Bessel beam trap but along the axis of the CRD standing wave (i.e. along z). The Bessel beam core radius is larger than the particle radius, and the gradient of the electromagnetic field is much lower than for other forms of optical traps such as optical tweezers generated by tight focusing of a laser beam using a microscope objective. The particle is therefore relatively free to undergo Brownian motion in the horizontal plane over distances of a few microns from the centre of the BB core. In these excursions, the particle samples nodes and anti-nodes of the standing wave associated with the cavity TEM_{00} mode, as well as regions between. Two further curves have therefore been added to figure 3 to show the predicted Q_{ext} measurements for a particle located at a node ($z = \lambda/4$) or an antinode ($z = 0$) of the cavity standing wave. These curves, which show the expected limits of deviation from plane wave Mie scattering, satisfactorily enclose most of the distribution of the experimental data points about the Mie scattering curve. It is apparent from this envelope in the distribution of the experimental extinction efficiency that the particle motion samples at least an entire wavelength of the TEM_{00} mode. The simulated curves pass more tightly through certain ranges of x_p and this behaviour is replicated in the experimental distribution of data points.

The calculated $\zeta(z)$ values plotted in figure 2 show that, for a particle at a fixed position relative to a standing wave, deviations of a few percent from the standard Mie calculation of extinction cross sections persist for size parameters as large as $x_p = 30$. However, the deviations can exceed 10% for $x_p < 20$, and are further enhanced if a single particle can move between axial (z) cavity positions corresponding to a node and an extremum of the intra-cavity field. Consider, for example, a particle moving along the cavity axis with speed $0.1\,\mathrm{m\,s^{-1}}$. The particle can traverse one or more wavelengths of the light over the timescale of a ring-down measurement, which commonly might exceed 10 μs. At each z-coordinate the particle presents a different effective extinction cross section so the ring-down intensity decay will not be a single exponential function of time. A standard exponential fit of the ring-down decay will therefore introduce further uncertainty into the determination of the optical properties of the particle, and hence scatter in the determined Q_{ext}

values. Confinement of a single particle along the z coordinate to sub-wavelength precision, as well as radially in the centre of the cavity mode, has not yet been demonstrated. However, the effects of non-single exponential ring down events on extinction efficiency retrievals were previously modelled and quantified.[10]

The example used here is a single component droplet, which simplifies the treatment of the refractive index in the Mie calculations of variation of Q_{ext} because a single value can be used for all particle sizes.   However, we have also observed very similar behaviour for particles with two components, such as aqueous NaCl droplets with the composition, and thus refractive index, changing with size. Again, the scatter in Q_{ext} measurements obtained by CRDS as the droplet size decreased (with reduction in ambient relative humidity) is accounted for by the random motion of the particle along the cavity axis, within the bounds imposed by the Bessel beam core.

5. Refractive index determination for a 1,2,6-hexanetriol droplet

Despite the effect of particle position on the experimental RDTs, the study of single accumulation mode aerosol particles by CRDS using our Bessel beam confinement method offers significant improvements in the precision of extinction cross section and refractive index determinations over multiple particle measurements on a flowing ensemble of size-selected aerosol.[14-15] Structure in the extinction efficiency resulting from resonances in the light scattering can be resolved, and provides precise constraints on the refractive index of the particle. In ensemble measurements, the averaging effect of the inevitable range of particle radii, even with initial size selection using a differential mobility analyser, smooths out much of this resonance structure. As we have shown here, the scatter in the single particle extinction measurements for a Bessel beam trapped particle is dominated by the lateral (z) motion of the particle in the optical trap. However, the limits of this scatter can quantitatively be accounted for by correct treatment of the interaction of a standing wave with the particle. Moreover, the envelope of scatter provides further information on the particle's optical properties because the refractive index is an input parameter to the calculation of ζ for different values of the size parameter. To demonstrate this concept, we computed Q_{ext} values as a function of x_p using limiting cases of $\zeta(z)$ with $z = 0$ and $\lambda/4$, and defined a figure of merit to be the fraction of the experimental data points that lie outside the envelope of these two calculated Q_{ext} curves. The calculations employed a value of the beam waist of the intra-cavity TEM$_{00}$ mode, which can be determined from the separation and radii of curvature of the mirrors, or can be included as a parameter in the data analysis.

A best fit value for the droplet RI was selected to correspond to the minimum in our figure of merit, using the following procedure. The radius of the particle was estimated every second by fitting an experimental phase function to a Mie-simulated phase function computed for an initially estimated and fixed refractive index. Each CRDS-measured σ_{ext} value can then be related to an estimated particle radius (and hence geometric cross-section). The evaluation of σ_{ext} from CRDS data requires a choice of TEM$_{00}$ cavity mode beam waist (equation (1)), which we included as a parameter in the analysis. We denote the initial refractive index and radius estimates by n_1 and r_1 respectively, and observe that the outcome of the fit did not depend on the starting choice of n_1. The true particle radius (r_2) and refractive index (n_2) satisfy the condition $r_1 n_1 = r_2 n_2$. Hence, by systematically varying n_2 (and consequently the corresponding r_2 value for each r_1), modified Mie simulations as per equation (2) could be compared to the experimental CRDS data, which were collected over a range of droplet radii, to obtain a best value of n_2. This analysis assumes that the refractive index is constant with droplet radius, and that droplet evaporation is sufficiently slow that its radius does not change during a CRDS measurement.

Figure 4 illustrates how the figure of merit changed with choice of refractive index and TEM$_{00}$ mode beam waist for analysis of the single-particle data shown in figure 3. The plot shows a region in which the merit function is a minimum. We took RI and w values from the midpoints between the contour line in figure 4 where the merit function rises above the baseline noise (shown as a thicker line in the figure). The fitting error in our refractive index determination for this particle was estimated using the distance from the chosen RI and w values to this contour line.
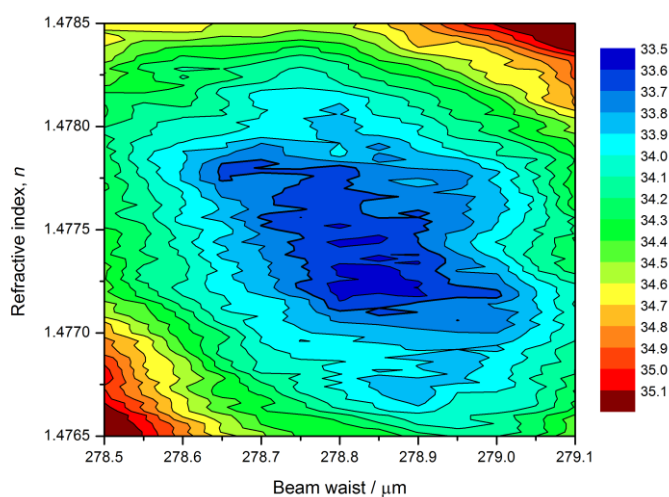

Figure 4: Variation of the number of experimentally determined Q_{ext} data points lying outside the envelope of modified Mie scattering curves obtained with $\zeta(z=0)$ and $\zeta(z=\lambda/4)$ with refractive index

9

input to the Mie calculations and beam waist (w) used in the analysis of the experimental data. The colour bar on the right quantifies the percentage of points lying outside this envelope. The thicker contour line was used to estimate fitting uncertainties.

The fitting procedure yielded a refractive index at λ = 532 nm of 1.47748 ± 0.0004 for the 1,2,6-hexanetriol particle for which experimental data are shown in figure 3. This value compares favourably (to ~0.1 %) to n_D^{20} = 1.4759 for pure 1,2,6-hexanetriol (99.9 %, Aldrich), as measured with a Misco digital refractometer at λ=589.3 nm   The beam waist derived from the analysis was 278.83 ± 0.18 μm. Repeat measurements for three further droplets of 1,2,6-hexanetriol gave RI values of 1.47920 ± 0.00070, 1.47840 ± 0.00021 and 1.47805 ± 0.00041, and beam waists of 276.42 ± 0.39, 277.66 ± 0.10 and 282.91 ± 0.10 μm. The uncertainty-weighted mean of the four RI value is 1.47824 ± 0.00072, with the uncertainty quoted as 1 SD of the 4 separate measurements because the (lower) uncertainties on individual determinations primarily reflect fitting errors. The 0.05 % (1 SD) precision in the refractive index implies a corresponding uncertainty in the determination of the droplet radius.

The refractive index at 532 nm is expected to be higher than that at 589.3 nm if the typical trend in dispersion is followed. However, incorporation of some water (with n_{532} = 1.335) into the hexanetriol droplet from moisture in the particle trapping cell (RH < 10 %) might have the opposite effect. We can also compare the retrieved refractive index to a recent and independent measurement for 1,2,6-hexanetriol droplets from our laboratory of n_{532} = 1.482 ± 0.001 (with 1 SD uncertainty).[16] This latter value was derived from a combination of phase function analysis and changes in the positions of evaporating particles subjected to radiation pressure from a Bessel beam and the Stokes drag force from a counter-propagating gas flow. The precisions in the RIs obtained from the two methods are similar, but the values lie just outside their mutual uncertainties. Nevertheless, the two values agree to within 0.25 %.

The rate of evaporation from the hexanetriol particle is sufficiently low that a trapped particle samples multiple positions within the ring-down cavity standing wave while maintaining a given radius. As figure 3 demonstrates, the envelope of extinction efficiency points is therefore well defined. However, our chosen fitting method to derive refractive index, using the percentage of measurements lying outside the expected Q_{ext} envelope, does not depend critically on this thorough sampling of particle positions. An alternative choice of fitting method might be to minimize the average absolute deviation of experimentally measured extinction efficiencies from the unmodified Mie simulation of $Q_{ext}(x_p)$ by varying the RI. This method would circumvent the calculation of $\zeta(z=0)$ and $\zeta(z=\lambda/4)$ phase parameters as a function of x_p for each RI value, but is based on a model that

does not correctly treat the scattering of the cavity standing wave by the particle. Care is also necessary in interpreting fits of any rolling average (or otherwise smoothed) version of the distribution of experimental Q_{ext} data points using uncorrected Mie scattering. The effects of different particle positions within the standing wave should average out if sufficient positions are sampled for a given particle radius, because, as is evident from figure 2, $\frac{1}{2}\left\{\zeta(z=0)+\zeta\left(z=\frac{\lambda}{4}\right)\right\}=1$ for any x_p. However, if the droplet radius change associated with evaporation (or condensation) is sufficiently fast, this averaging may be incomplete at a given size parameter

6. Conclusions

We have demonstrated that a combination of Bessel beam confinement and manipulation of a single particle with CRDS measurement of optical extinction can provide very precise determination of refractive index for accumulation mode aerosol particles. The Brownian motion of the particle within the core of the Bessel beam results in a distribution of extinction efficiency values because the particle samples different regions of the standing wave of the intra-cavity probe laser light. However, quantitative analysis of the envelope of this distribution of Q_{ext} can be used to advantage to improve the accuracy and precision of evaluation of the particle radius and refractive index. From measurements for four evaporating droplets of 1,2,6-hexanetriol, we determine a mean refractive index of 1.47824 ± 0.00072 at a wavelength of 532 nm.

References

1.   *Climate Change 2013: The Physical Science Basis. IPCC 5th Assessment Report*. 2013.
2.   Davies, J. F.; Haddrell, A. E.; Miles, R. E. H.; Bull, C. R.; Reid, J. P., Bulk, Surface, and Gas-Phase Limited Water Transport in Aerosol. *J. Phys. Chem. A* **2012**, *116* (45), 10987-10998.

3. Dennis-Smither, B. J.; Miles, R. E. H.; Reid, J. P., Oxidative Aging of Mixed Oleic Acid/Sodium Chloride Aerosol Particles. *J. Geophys. Res.-Atmos.* **2012,** *117*.

4. Krieger, U. K.; Marcolli, C.; Reid, J. P., Exploring the Complexity of Aerosol Particle Properties and Processes Using Single Particle Techniques. *Chem. Soc. Rev.* **2012,** *41* (19), 6631-6662.

5. Tang, I. N., Thermodynamic and Optical Properties of Mixed-Salt Aerosols of Atmospheric Importance. *J. Geophys. Res.-Atmos.* **1997,** *102* (D2), 1883-1893.

6. Tang, I. N.; Munkelwitz, H. R., Water Activities, Densities, and Refractive-Indexes of Aqueous Sulfates and Sodium-Nitrate Droplets of Atmospheric Importance. *J. Geophys. Res.-Atmos.* **1994,** *99* (D9), 18801-18808.

7. Walker, J. S.; Carruthers, A. E.; Orr-Ewing, A. J.; Reid, J. P., Measurements of Light Extinction by Single Aerosol Particles. *J. Phys. Chem. Lett.* **2013,** *4* (10), 1748-1752.

8. Butler, T. J. A.; Miller, J. L.; Orr-Ewing, A. J., Cavity Ring-Down Spectroscopy Measurements of Single Aerosol Particle Extinction. I. The Effect of Position of a Particle within the Laser Beam on Extinction. *J. Chem. Phys.* **2007,** *126* (17), 174302.

9. Siegman, A. E., *Lasers*. University Science Books: Sausalito, California, 1986.

10. Miller, J. L.; Orr-Ewing, A. J., Cavity Ring-Down Spectroscopy Measurement of Single Aerosol Particle Extinction. II. Extinction of Light by an Aerosol Particle in an Optical Cavity Excited by a CW Laser. *J. Chem. Phys.* **2007,** *126* (17), 174303.

11. Barnes, M. D.; Lermer, N.; Whitten, W. B.; Ramsey, J. M., CCD Based Approach to High-Precision Size and Refractive Index Determination of Levitated Microdroplets Using Fraunhofer Diffraction. *Rev. Sci. Instrumen.* **1997,** *68* (6), 2287-2291.

12. Carruthers, A. E.; Walker, J. S.; Casey, A.; Orr-Ewing, A. J.; Reid, J. P., Selection and Characterization of Aerosol Particle Size Using a Bessel Beam Optical Trap for Single Particle Analysis. *Phys. Chem. Chem. Phys.* **2012,** *14* (19), 6741-6748.

13. Mie, G., Articles on the Optical Characteristics of Turbid Tubes, Especially Colloidal Metal Solutions. *Ann. Physik* **1908,** *25* (3), 377-445.

14. Miles, R. E. H.; Rudic, S.; Orr-Ewing, A. J.; Reid, J. P., Sources of Error and Uncertainty in the Use of Cavity Ring Down Spectroscopy to Measure Aerosol Optical Properties. *Aerosol Sci. Technol.* **2011,** *45* (11), 1360-1375.

15. Mason, B. J.; King, S. J.; Miles, R. E. H.; Manfred, K. M.; Rickards, A. M. J.; Kim, J.; Reid, J. P.; Orr-Ewing, A. J., Comparison of the Accuracy of Aerosol Refractive Index Measurements from Single Particle and Ensemble Techniques. *J. Phys. Chem. A* **2012,** *116* (33), 8547-8556.

16. Cotterell, M. I.; Mason, B. J.; Carruthers, A. E.; Walker, J. S.; Orr-Ewing, A. J.; Reid, J. P., Measurements of the Evaporation and Hygroscopic Response of Single Fine-Mode Aerosol Particles Using a Bessel Beam Optical Trap. *Phys. Chem. Chem. Phys.* **2014,** *16* (5), 2118 - 2128.

Table of Contents Graphic